FINDING ROBUST MINIMIZER FOR
NON-CONVEX PHASE RETRIEVAL

Tingting Wu[✉1], Chaoyan Huang[✉2], Xiaoyu Gu[✉1],
Jianwei Niu[✉2] and Tieyong Zeng[✉*2]

[1]School of Science, Nanjing University of Posts
and Telecommunications, Nanjing, China

[2]Department of Mathematics,
The Chinese University of Hong Kong, Shatin, N. T., Hong Kong, China

(Communicated by Yifei Lou)

ABSTRACT. The phase retrieval task has received considerable attention in recent years. Here, phase retrieval refers to the problem of recovering the clear image from magnitude-only data of its Fourier transform, or other linear transforms. As the observed magnitude signal is usually corrupted by heavy noise, retrieving the original object is rather difficult. In this paper, we investigate a regularization-based framelet method to recover the phase information and alleviate the influence of noise. Indeed, since phase retrieval is usually modeled by a non-convex model, how to find the solution efficiently is an intricate challenge. For this reason, we first reformulate the objective function as the difference between two convex functions. By introducing the boosted difference of convex algorithm (BDCA), the proposed scheme has good performance in handling the phase retrieval problem. Theoretically, we also present the convergence analysis of the numerical algorithm. To exhibit the effectiveness of our approach, we consider two classical regularizers with the proposed framework. Besides, two different measurement models are carefully studied to illustrate the robustness of our scheme. Numerical experiments demonstrate clearly that the proposed framelet method is effective and robust in tackling the non-convex phase retrieval task.

1. **Introduction.** In optics, the information on high-frequency light waves can be readily recorded by optical devices. However, obtaining the phase information of these lights is quite difficult. The reason is that the diffraction pattern can only capture the absolute value of the Fourier transformed sample [25]. Furthermore, the observed magnitude is frequently corrupted by heavy noise during the signal acquisition process, which makes the image recovery problem more complicated.

Since the phase of an image contains rich information, it is important to reconstruct the latent image efficiently. In the literature, phase retrieval has been widely utilized in adaptive optics [22], inverse problem [26], and optical imaging [39].

The main point of phase retrieval is to consider how to recover an image or a signal from its Fourier-transformed magnitude with heavy noise. In the past decades, various remarkable methods have been applied to handle the phase retrieval task with or without the regularizer. For example, the Gerchberg-Saxton algorithm (also called the error-reduction algorithm) was originally proposed to handle the phase retrieval problem [21]. Through the straightforward transform between the Fourier and real domain, the phase can be well reconstructed. In [9], Candes, Li, and Soltanolkotabi suggested a Wirtinger flow (WF) algorithm to solve a non-convex model of the phase retrieval problem with careful initialization. In [33], Netrapalli, Jain, and Sanghavi used spectral initialization of WF for the error reduction algorithm. Moreover, Wang et al. [49] proposed a sparse truncated amplitude flow algorithm (SPARTA) with low computational complexity to reconstruct a signal. In [46], Vaswani, Nayer, and Eldar handled the low-rank phase retrieval problem by modifying the truncated Wirtinger flow (TWF) [15] and alternating minimization technique. There are many other methods proposed for phase retrieval, such as the PhaseLift method [7], the difference map iterative scheme [18], the hybrid input-output (HIO) algorithm [19], PhaseLamp [16], and so on. The interested readers are referred to [55] for a comprehensive review.

The methods mentioned above are efficient for reconstructing the latent image from the magnitudes of the Fourier-transformed signal. Considering that phase retrieval is an ill-posed problem and the obtained images are probably being corrupted by the heavy noise [11], a regularization term should be applied to better suppress noise. The classic regularizers include the total variation regularizer [37], tight frame function [56], and low-rank regularizer [45], etc. More specifically, a tight frame model that took advantage of the signal's sparsity with support prior was proposed to solve the phase retrieval problem [40]. Chang et al. [11] introduced a total variation-based model to reconstruct an image from its noisy magnitude. In [29], a phase retrieval model with the low-rank regularizer based on the Bayesian framework was proposed. Although regularizers helped in reconstructing the image, the phase retrieval problem is still non-convex and the optimization methods may converge to some local minimizers [41]. Besides, different initial values probably generate different solutions. Therefore, how to efficiently find a good solution to the phase retrieval task is still an open question.

In the literature, many excellent algorithms have been proposed to solve the non-convex image processing problem, such as [12]. Specifically, an effective algorithm [6] was proposed for phase retrieval, which converges under certain conditions. In [35], the low-complexity algorithms with a superior performance based on the majorization-minimization (MM) framework was proposed to handle the phase retrieval problem. In [34], the proximal alternating linearization algorithm was employed to handle the phase retrieval model. However, the convergence of their algorithm was guaranteed under some assumptions. Hence, it is difficult to find the robust minimizer of the phase retrieval task under some general cases. Note that a novel algorithm named the boosted difference of convex functions algorithm (BDCA) [3] was proposed to tackle non-smooth functions. The DCA is a special case of MM algorithm. In this paper, the boost DCA is considered to tackle the phase retrieval task. The improvement of a more general case of MM algorithm

will be considered in the future. The details of the BDCA are presented in Section 3. By ameliorating the DCA with a line search step along the descent direction, the BDCA is four times faster than the related methods [1] in both iterations and computational time. Besides, it has been proved that every cluster point of the BDCA is a stationary point [3]. However, not many works applied the BDCA in data science and the effectiveness of this algorithm is still debatable. In this paper, we try to address the BDCA to solve the proposed model and give the convergence analysis.

Indeed, considering that various works have ignored the effect of noise and the non-convex property, in this paper, we propose a general regularization framework for phase retrieval with Gaussian noise. We test our approach with two basic and effective regularizers: total variation (TV) and tight frame (TF). For the optimization scheme, we first reformulate the model to be strongly convex with the Huber function [24] and a square term. Then we introduce the BDCA to solve the new proposed model with guaranteed convergence. Furthermore, we also test with two different measurements ($3n$ Fourier and coded diffraction pattern) to demonstrate the robustness of the proposed approach. Experiment results imply that our strategy is flexible and effective with convergence for different regularization terms and measurements on the phase retrieval task.

The paper is organized as follows. Mathematical models are given in Section 2; a brief review of the BDCA is given in Section 3; our model and theoretical analysis are given in Section 4; experimental results are given in Section 5; and Section 6 follows the conclusion.

2. **Mathematical models.** In this section, the mathematical models of the phase retrieval task are reviewed. Firstly, the basic definitions are presented. Secondly, the general acquisition process is described. Thirdly, a brief review of the regularizer-based phase retrieval model is presented.

2.1. **Basic mathematical notions.** In order to increase the readability of the paper, we give some basic mathematical definitions.

Definition 2.1 (convex function)**.** Let X be a convex subset of a real vector space and let $f : X \to \mathbb{R}$ be a function. Then f is called **convex** if and only if any of the following equivalent conditions hold:

1. For all $0 \le t \le 1$ and all $x_1, x_2 \in X$:
$$f\left(tx_1 + (1-t)x_2\right) \le tf\left(x_1\right) + (1-t)f\left(x_2\right);$$

2. For all $0 < t < 1$ and all $x_1, x_2 \in X$ such that $x_1 \ne x_2$:
$$f\left(tx_1 + (1-t)x_2\right) \le tf\left(x_1\right) + (1-t)f\left(x_2\right).$$

Remark 2.2 (non-convex)**.** A function is **non-convex** if the function is not a convex function.

Definition 2.3 (strongly convex)**.** A differentiable function f is **strongly convex** if
$$f(y) \ge f(x) + \langle h, y - x \rangle + \frac{\mu}{2}\|y - x\|^2$$
for some $\mu > 0$, $h \in \nabla f(x)$, and all x, y.

Definition 2.4 (coercive)**.** An (extended valued) function $f : \mathbb{R}^n \to \mathbb{R} \cup \{-\infty, +\infty\}$ is called **coercive** if
$$f(x) \to +\infty \text{ as } \|x\| \to +\infty.$$

Definition 2.5 (subgradient). g is a **subgradient** of a convex function f at $x \in$ dom f if

$$f(y) \geq f(x) + \langle g, y - x \rangle, \quad \forall y \in \text{dom } f,$$

where dom $f = \{x \in X : f(x) < +\infty\}$.

2.2. **Phase retrieval problem.** Assume that $\mathbb{C}$ is the complex domain, by representing a two-dimensional image in terms of a vector by the lexicographical order, i.e., let $u : \Omega = \{0, 1, ..., n_1 \times n_2 - 1\} \to \mathbb{C}$ of size $n = n_1 \times n_2$ be the two-dimensional ground truth image on a discrete lattice. Denote $\mathcal{F} : \mathbb{C}^n \to \mathbb{C}^n$ as the discrete Fourier transform (DFT)

$$\mathcal{F}u\left(\omega_1 + \omega_2 n_1\right) := \frac{1}{\sqrt{n}} \sum_{0 \leq t_j \leq n_j - 1} u\left(t_1 + t_2 n_1\right) \exp\left(-2\pi\mathbf{i}\left(\frac{\omega_1 t_1}{n_1} + \frac{\omega_2 t_2}{n_2}\right)\right), \quad (1)$$

where $\forall \, 0 \leq \omega_j \leq n_j - 1$ for $j = 1, 2$, and $\mathbf{i} = \sqrt{-1}$ is the imaginary unit. Then the obtained data is the absolute value of the Fourier transformed u, *i.e.*, $|\mathcal{F}u|$, where $|\cdot|$ means the absolute value operator. In fact, the DFT can be replaced with an arbitrary linear operator $\mathcal{A}$ [11], leading to a general phase retrieval problem as follows

$$\min_u \||\mathcal{A}u| - b\|^2, \quad (2)$$

where the observed image $b : \Lambda = \{0, 1, \ldots, m - 1\} \to \mathbb{R}_+$, $\mathcal{A} : \mathbb{C}^n \to \mathbb{C}^m$ $(m > n)$ is a linear operator in the complex Euclidean space, and $\|\cdot\|$ is the Euclidean norm. Eq. (2) denotes the minimum value of the objective function $f(u) = \||\mathcal{A}u| - b\|^2$ when choosing u from the set of the complex domain. A vector $u^\star$ is called optimal, or a solution of the problem (2), if it has the smallest objective value, i.e., $f(u) \geq f(u^\star)$, $\forall \, u$ from the given domain [5].

In the literature, there are many types of measurements. For example, Candès et al. [7] proved exact phase retrieval from $3n$ Fourier measurements is effective, where

$$\mathcal{A}u = \begin{bmatrix} \mathcal{F}u \\ \mathcal{F}\left(u + \mathscr{D}^{s_1,s_2}u\right) \\ \mathcal{F}\left(u - \mathbf{i}\mathscr{D}^{s_1,s_2}u\right) \end{bmatrix}, \quad (3)$$

and $\left(\mathscr{D}^{s_1,s_2}u\right)(t_1 + t_2 n_1) = \exp\left(\frac{2\pi\mathbf{i}s_1 t_1}{n_1} + \frac{2\pi\mathbf{i}s_2 t_2}{n_2}\right) u\left(t_1 + t_2 n_1\right)$, $0 \leq t_j \leq n_j - 1$, here integers s_1, s_2 coprime to n_1, n_2, respectively. Many researchers applied Eq.(3) to simulate phase retrieval degradation [11, 17]. Later, an effective measurement of coded diffraction pattern (CDP) [8, 14] was proposed as

$$\mathcal{A}u = \begin{bmatrix} \mathcal{F}(I_1) \circ u \\ \mathcal{F}(I_2) \circ u \\ \vdots \\ \mathcal{F}(I_r) \circ u \end{bmatrix}, \quad (4)$$

where $\circ$ is the Hadamard product and $I_1, \cdots, I_r \in \mathbb{C}^n$ are diagonal matrices. We take both Eq.(3) and Eq.(4) into consideration to illustrate the robustness of our scheme.

2.3. **Phase retrieval models.** From model (2), it is apparent that without prior information, there is no unique solution of u. The main goal of phase retrieval is to achieve an efficient algorithm that recovers data with minimal errors and is stable in the case of heavy noise. In the past decades, many researchers have developed

various practical numerical algorithms by exploring the characteristics and internal structure of signals according to specific problems.

In [40], the authors developed a translation invariant Haar pyramid tight frame regularizer with the support prior for sparse phase retrieval. They assumed that the magnitude is corrupted by the Gaussian white noise ζ with zero mean, $i.e.$, $b = |\mathcal{A}u| + \zeta$. Their model was written as

$$\min_{0 \leq u \leq 1} \frac{\lambda}{2} \||\mathcal{A}u| - b\|^2 + \|\mathcal{W}u\|_1, \tag{5}$$

where $\mathcal{A}$ is the DFT matrix, λ is a positive parameter, $\|x\|_1 = \sum_{i=1}^n |x_i|$ is the ℓ_1-norm with $x = (x_1, x_2, \cdots, x_n)$, and $\mathcal{W}$ denotes the translation invariant Haar pyramid tight frame operator, which satisfies $\mathcal{W}^T \mathcal{W} = \mathcal{I}$ (here $\mathcal{I}$ is an identity matrix). The authors applied the alternating direction method of multipliers (ADMM) scheme [13, 20] to solve model (5) which is a non-convex problem. The optimal solution of each subproblem exists. However, the convergence to the solution is not guaranteed. In addition, the DFT matrix can not describe the degradation process of phase acquisition exactly [7].

In [11], the total variation regularization was adopted to phase retrieval problem with Gaussian noise. Besides, the $3n$ Fourier measurements as in Eq.(3) were used to describe $\mathcal{A}u$. The model was written as

$$\min_{0 \leq u \leq 1} \frac{\lambda}{2} \||\mathcal{A}u| - b\|^2 + \|\nabla u\|_1, \tag{6}$$

where ∇ is the discrete gradient operator as $(\nabla u)_{i,j} = \left(\left(\nabla_x^+ u\right)_{i,j}, \left(\nabla_y^+ u\right)_{i,j} \right)$ and (i, j) denotes a pixel of the image with

$$\begin{aligned}
\left(\nabla_x^+ u\right)_{i,j} &:= \begin{cases} u_{i,j+1} - u_{i,j}, & 1 \leq j \leq n_1 - 1, \\ 0, & j = n_1, \end{cases} \\
\left(\nabla_y^+ u\right)_{i,j} &:= \begin{cases} u_{i+1,j} - u_{i,j}, & 1 \leq i \leq n_2 - 1, \\ 0, & i = n_2. \end{cases}
\end{aligned} \tag{7}$$

The total variation regularization has good properties of keeping the edge and helps to generate better phase reconstruction results. The author handled Eq.(6) with the ADMM algorithm and the convergence of u is still without guarantee. The phase retrieval model is a typical non-convex problem. Although the ADMM algorithm can be used to solve the model, the robust minimizer is not guaranteed. Since the BDCA can well handle the non-convex model, we use a deformation of our model to make it easy to solve under the framework of the BDCA. The BDCA is relatively new and rarely emerges in image science. For better illustration, we will give a brief review of the BDCA in the next section.

3. **A brief review of BDCA.** In fact, there are many prominent algorithms for the non-convex minimization problem. One of the popular algorithms is the BDCA. In this section, we present a brief review of the BDCA. The DC theory was created in 1986 [42], and extended by [23, 43]. Many works were devoted to promoting the progression of the DC theory, such as [38, 51]. Among these works, Artacho et al. [2, 3] boosted the convergence rate of the DC algorithm by adding a line search step along the descent direction. Given a function $F : \mathbb{R}^n \to \mathbb{R} \cup \{+\infty\}$, we need to solve $\inf F(u) : u \in \mathbb{R}^n$. The DC algorithm substitutes F by a difference between

functions G and H, which are two lower semi-continuous proper convex functions, such that

$$F(u) = G(u) - H(u), \quad \forall u \in \mathbb{R}^n. \tag{8}$$

The DC algorithm is based on convex analysis and primal-dual theory. Its key idea is to extend the convex analysis to non-smooth and non-convex analysis with convex programming. The primal problem is

$$\inf_{u \in \mathbb{R}^n} F(u) = \inf_{u \in \mathbb{R}^n} (G(u) - H(u)), \tag{9}$$

where $\inf_{u \in \mathbb{R}^n} F(u)$ is to find the infimum of $F(u)$ by choosing u in the set of $\mathbb{R}^n$. Some properties [43] of the DC algorithm are summarized in Definition 3.1. The main idea of DCA is simple: each iteration k of DCA approximates the concave part $-H$ by its affine majorization (that corresponds to taking $\mathbf{y}^k \in \partial H\left(\mathbf{u}^k\right)$) and computes $\mathbf{u}^{k+1}$ by solving the resulting convex problem, $\min_u \left\{ G(\mathbf{x}) - \left\langle \mathbf{u}, \mathbf{y}^k \right\rangle : \mathbf{u} \in \mathbb{R}^n \right\}$.

Definition 3.1. For the primal DC program, u^* is called a critical point of $G(u) - H(u)$ or generalized Karush-Kuhn-Tucker (KKT) point for (9) if $\partial H\left(u^*\right) \cap \partial G\left(u^*\right) \neq \emptyset$ and $\emptyset \neq \partial H\left(u^*\right) \subset \partial G\left(u^*\right)$.

In the DC theory [43], Tao and An have proved that the critical point u^* is a local minimum for non-convex function $F(u)$. The convergence property of the DC algorithm is also discussed in their study. The BDCA is the extension of DCA, where the function F is non-differentiable. Significantly, the version used in this paper restricts that G is differentiable and H is non-differentiable [3]. The line search is employed along the descent direction (generated by DCA) and the BDCA can be described as Algorithm 1, in which $d^k = y^k - u^k$ is a descent direction for $F(u)$ at y^k. We can choose the initial value $\bar{\beta}_k > 0$ freely in the line search step used for finding an appropriate value of the step size β_k. Meanwhile, we need to mention that the iterations of the BDCA and the DCA coincide when $\bar{\beta}_k = 0$. The other core idea of the DC algorithm is for minimization of the difference $G(u) - H(u)$ as Eq. (8), first H is replaced by its first order approximation $H\left(u^0\right) + \left\langle u - u^0, h^0 \right\rangle$, where h^0 is a vector in subgradient of H at point u^0 in Algorithm 1. Then, $G(u) - H\left(u^0\right) - \left\langle u - u^0, h^0 \right\rangle$ is a convex function and can be optimized efficiently.

4. **The proposed regularizer framelet method.** In this paper, we propose a general regularizer framework to handle the phase retrieval problem. Two different regularizers and two different measurements are applied to demonstrate the effectiveness of our strategy.

We assume the original image u is non-negative, bounded, and real-valued. The proposed scheme can be formulated as

$$\min_u \frac{\lambda}{2} \||\mathcal{A}u| - b\|^2 + \Phi(u), \tag{10}$$

where λ is a positive parameter; b is the observed image; $\mathcal{A}$ is a linear operator, two kinds of measurements ($3n$ Fourier measurements and CDP) are applied; and $\Phi(u)$ is the regularization term. We apply two different regularizers: the total variation regularizer $\|\nabla u\|_1$ and the tight frame regularizer $\|\mathcal{W}u\|_1$ to demonstrate the robustness of the proposed model. Here $\|x\|_1 = \sum_t^l |x_t|$ with $\{x = x_1, x_2, \cdots, x_l\}$. Since those two regularizers are related to the ℓ_1 norm, we introduce the Huber function [24, 27] to smooth the ℓ_1 norm. The Huber function $\Phi_\epsilon(u) = \sum_{i=1}^n \Psi_\epsilon(u_i)$

Algorithm 1 Boosted DC algorithm

Initialization $u^0 \in \mathbb{R}^n$, $\alpha > 0$, $0 < \xi < 1$, $m = 0$, $k = 0$, ϵ_1, ϵ_2

for $\frac{\|u^{k+1}-u^k\|}{\|u^k\|} \leq \epsilon_1$ **do**

  Calculate h^k by $h^k \in \partial H\left(u^k\right)$

  for $\frac{\|u^{m+1}-u^m\|}{\|u^m\|} \leq \epsilon_2$ **do**

    Calculate u^{m+1} by $u^{m+1} \in \arg\min_u \left\{ G(u) - \left[H\left(u^m\right) + \left\langle u - u^m, h^k \right\rangle \right] \right\}$

  end for

  Set $y^k = u^{m+1}$, $d^k = y^k - u^k$

  if $d^k = 0$ **then**

    Stop and return u^k

  else

    Choose any $\bar{\beta}_k > 0$ and set $\beta_k = \bar{\beta}_k$

    while $F\left(y^k + \beta_k d^k\right) > F\left(y^k\right) - \alpha \beta_k{}^2 \left\|d^k\right\|^2$ **do**

      $\beta_k = \xi \beta_k$

    end while

    Set $u^{k+1} = y^k + \beta_k d^k$

    if $u^{k+1} = u^k$ **then**

      Stop and return u^k

    end if

  end if

end for

---

can be seen as the Moreau-Yosida regularization [28] of the ℓ_1 norm and has the following form

$$\Phi_\epsilon(u) = \sum_{i=1}^{n} \Psi_\epsilon(u_i) \quad \text{with} \quad \Psi_\epsilon(u_i) = \inf_t \left\{ \Phi(t) + \frac{1}{2\epsilon} |u_i - t|^2 \right\} = \begin{cases} \dfrac{1}{2\epsilon} |u_i|^2, & |u_i| \leq \epsilon, \\ |u_i| - \dfrac{\epsilon}{2}, & |u_i| > \epsilon, \end{cases} \tag{11}$$

where $\epsilon > 0$, $\Phi_\epsilon(u)$ is continuously differentiable and

$$\nabla \Psi_\epsilon(u_i) = \begin{cases} \dfrac{1}{\epsilon} u_i, & |u_i| \leq \epsilon, \\ \text{sign}(u_i), & |u_i| > \epsilon. \end{cases} \tag{12}$$

The minimizer of $\Phi_\epsilon(u)$ and $\Phi(u)$ are the same, and we refer the interested readers to [31, 32] for a comprehensive review. The model (10) favors the solution being approximately piece-wise constant, and the model is effective for the data corrupted by the Gaussian white noise. In addition, the existence of the minimizer (10) is also proved ([11], Theorem 3.1).

Proposition 4.1. *Denote Ω as the bounded and Lipschitz-regular domain, and given non-negative data $b = (b_0, b_1, b_2)$, then model (10) has at least one minimizer $u^* \in BV(\Omega)$.*

By applying the BDCA, we first reformulate the proposed model (10) as

$$\min_{0 \leq u \leq 1} F(u) = \min_u \Phi_\epsilon(u) + \frac{\lambda}{2} \|| \mathcal{A}u\||^2 - \lambda \langle b, |\mathcal{A}u| \rangle, \tag{13}$$

where $\langle \cdot, \cdot \rangle$ is the complex inner product. Hence $F(u)$ can be split to $G(u)$ and $H(u)$ naturally, *i.e.*,

$$
\begin{aligned}
G(u) =& \Phi_\epsilon(u) + \frac{\lambda}{2}\||\mathcal{A}u|\|^2 + \frac{\rho}{2}\|u\|^2, \\
H(u) =& \lambda\langle b, |\mathcal{A}u| \rangle + \frac{\rho}{2}\|u\|^2,
\end{aligned}
\tag{14}
$$

where convexity of $H(u)$ is due to entries of b being non-negative, and modulus ρ is a positive constant to make the components $G(u)$ and $H(u)$ strongly convex. Based on the framework of BDCA, we need to find out $h^k \in \partial H(u^k)$. Since $H(u)$ is non-smooth, we have the following formula

$$
h^k = \lambda \mathcal{A}^*(b \circ \text{sign}(\mathcal{A}u^k)) + \rho u^k,
\tag{15}
$$

where $\mathcal{A}^*$ is the conjugate transpose of $\mathcal{A}$, and $\text{sign}(\cdot)$ is the sign function applying to a vector element-wisely [11]. Then we have

$$
\begin{aligned}
u^{k+1} &= \arg\min_u G(u) - \langle h^k, u \rangle \\
&= \arg\min_u \Phi_\epsilon(u) + \frac{\lambda}{2}\||\mathcal{A}u|\|^2 + \frac{\rho}{2}\|u\|^2 - \langle h^k, u \rangle.
\end{aligned}
\tag{16}
$$

For the total variation regularizer and the tight frame regularizer, it is not difficult to find that the only difference is the operator $\mathcal{W}$ and ∇. For simplicity, we denote $\mathcal{B}$ as the operator $\mathcal{W}$ or ∇, *i.e.*, $\Phi(u) = \|\mathcal{B}u\|_1$. Based on the ADMM algorithm, we rewrite the above equation (16) as follows

$$
\begin{aligned}
\min_u \quad & \Phi_\epsilon(u) + \frac{\lambda}{2}\||z|\|^2 + \frac{\rho}{2}\|u\|^2 - \langle h^k, u \rangle, \\
\text{s.t.} \quad & z = \mathcal{A}u, \quad v = u, \quad p = \mathcal{B}u,
\end{aligned}
\tag{17}
$$

where $z = (z_0, z_1, z_2)$.

To clarify downsampling for $3n$ Fourier measurements Eq.(3), we introduce three subsets: $\Omega_i \subset \Omega$, for $i = 0, 1, 2$, each of which provides a binary mask of the incomplete Fourier transform magnitude. One can readily construct the augmented Lagrangian function as

$$
\begin{aligned}
&\mathcal{L}_{r_1, r_2, r_3}(p, u, v, z; w, q, d) \\
&= \Phi_\epsilon(u) + \frac{\lambda}{2}\||z|\|^2 + \frac{\rho}{2}\|u\|^2 - \langle h, u \rangle + \langle z - \mathcal{A}u, d \rangle \\
&+ \langle p - \mathcal{B}u, q \rangle + \langle u - v, w \rangle + \frac{r_1}{2}\|z - \mathcal{A}u\|^2 + \frac{r_2}{2}\|u - v\|^2 + \frac{r_3}{2}\|p - \mathcal{B}u\|^2,
\end{aligned}
\tag{18}
$$

where w, q, d are called Lagrange multipliers or dual variables and r_1, r_2, r_3 are Lagrange penalty parameters. Alternating minimization for the above Lagrangian consists of solving four subproblems *w.r.t.* p, u, v and z, followed by updating dual variables. Below we elaborate on solving each subproblem with m-th iteration.

4.1. **v-subproblem.** The v-subproblem is

$$
v^{m+1} = \arg\min_v \langle u^m - v^m, w^m \rangle + \frac{r_2}{2}\|u^m - v^m\|^2,
\tag{19}
$$

which has a closed solution as follows

$$
v^{m+1} = \min\{1, \max\{0, u^m + \frac{w^m}{r_2}\}\}.
\tag{20}
$$

4.2. **P-subproblem.** We can expand the objective function of the p-subproblem as

$$\Phi_\varepsilon(p) + \langle p - \mathcal{B}u^m, q^m \rangle + \frac{r_3}{2} \|p - \mathcal{B}u^m\|^2$$

$$= \sum_{j=0}^{2n-1} \left[\Psi_\varepsilon(p_j) + q_j^m \left(p_j - (\mathcal{B}u^m)_j \right) + \frac{r_3}{2} \left(p_j - (\mathcal{B}u^m)_j \right)^2 \right]$$

and solve the minimization for each j separately. Let $\hat{p} = \mathcal{B}u - \dfrac{q}{r_3}$, we have the solution with soft-shrinkage algorithm as

$$p_j^{m+1} = \hat{p}_j^m - \frac{\frac{1}{r_3}\hat{p}_j^m}{\max\{\frac{1}{r_3} + \epsilon, \|\hat{p}_j^m\|\}}. \tag{21}$$

4.3. **Z-subproblem.** Suppose for $3n$ Fourier measurement (3), minimization for each component of $z = (z_0, z_1, z_2)$ is independent of the other two, so we just describe how to solve for z_0 as an example. Note that here z_0 is a vector and we apply all operations entrywise. The z_0-subproblem is

$$z_0^{m+1} = \arg\min_{z_0} \frac{\lambda}{2} \||z_0^m|\|^2 + \langle z_0^m - \mathcal{A}u^m, d_0 \rangle + \frac{r_1}{2} \|z_0^m - \mathcal{A}u^m\|^2. \tag{22}$$

We can decompose the minimization problem

$$z_0^{m+1} = \arg\min_{z_0} \frac{\lambda}{2} |z_0^m|^2 + \frac{r_1}{2} \left| z_0^m - \mathcal{A}u^m + \frac{d_0}{r_1} \right|^2$$

$$= \arg\min_{z_0} \frac{\lambda}{2} |z_0^m|^2 + \frac{r_1}{2} \left[|z_0^m|^2 + \left| \mathcal{A}u^m - \frac{d_0}{r} \right|^2 - 2|z_0^m| \operatorname{Re} \left(\operatorname{sign}(z_0^m) \left(\overline{\mathcal{A}u^m - \frac{d_0}{r}} \right) \right) \right] \tag{23}$$

into two subproblems, *i.e.*, $|z_0|$ and $\operatorname{sign}(z_0)$ ($\operatorname{sign}(z_0) = \frac{z_0}{|z_0|}$ if $z_0 \neq 0$; otherwise $\operatorname{sign}(0) = c$ with an arbitrary constant $c \in \mathbb{C}$ with unity length). One can readily obtain $\operatorname{sign}(z_0^m) = \operatorname{sign}(\mathcal{A}u^m - \frac{d_0}{r})$. To minimize the subproblem $|z_0|$, we have

$$\left| z_0^{m+1} \right| = \arg\min_{|z_0| \in \mathbb{R}_+} \frac{\lambda}{2} |z_0^m|^2 + \frac{r_1}{2} \left(|z_0^m| - \left| \mathcal{A}u^m - \frac{d_0}{r_1} \right| \right)^2, \tag{24}$$

which has a closed-form solution

$$\left| z_0^{m+1} \right| = \frac{r_1 \left| \mathcal{A}u^m - \dfrac{d_0^m}{r_1} \right|}{\lambda + r_1}. \tag{25}$$

Letting $\delta^m = \mathcal{A}u^m - d_0^m / r_1$, we reformulate the above solution as

$$z_0^{m+1} = \frac{r_1 |\delta^m|}{\lambda + r_1} \operatorname{sign}(\delta^m). \tag{26}$$

For the CDP measurement (4), the r-components $\mathcal{F}(I_j) \circ u, j = 1, 2, \cdots, r$, where $\circ$ is the Hadamard product and $I_1, \cdots, I_r \in \mathbb{C}^n$ are diagonal matrices. Then z-subproblem is with r components, similar to Eq. (22), we can get the solution of p-subproblem of the CDP measurement.

4.4. **U-subproblem.** At last, we consider u-subproblem

$$u^{m+1} = \arg\min_u \frac{\rho}{2}\|u^m\|^2 - \langle h^k, u^m \rangle + \langle z^{m+1} - \mathcal{A}u^m, d^m \rangle$$
$$+ \langle p^{m+1} - \mathcal{B}u^m, q^m \rangle + \langle u^m - v^{m+1}, w^m \rangle + \frac{r_1}{2}\|z^{m+1} - \mathcal{A}u^m\|^2 \quad (27)$$
$$+ \frac{r_2}{2}\|u^m - v^{m+1}\|^2 + \frac{r_3}{2}\|p^{m+1} - \mathcal{B}u^m\|^2.$$

According to Eq.(3), by computing the derivative of $\|z - \mathcal{A}u\|^2/2$ as follows

$$\partial_u\left(\|z_0 - \mathcal{F}u\|^2/2\right) = \partial_u\left(\|\mathcal{F}^*z_0 - u\|^2/2\right) = u - \Re(\mathcal{F}^*z_0), \quad (28a)$$

$$\partial_u\left(\|z_1 - \mathcal{F}\left(u + \mathscr{D}^{s_1,s_2}u\right)\|^2/2\right) = (2 + 2\Re(\mathscr{D}^{s_1,s_2}))u - \Re(\mathcal{F}^*z_1 + \mathscr{D}^{s_1,s_2}\overline{\mathcal{F}^*z_1}), \quad (28b)$$

$$\partial_u\left(\|z_2 - \mathcal{F}\left(u - \mathbf{i}\mathscr{D}^{s_1,s_2}u\right)\|^2/2\right) = (2 + 2\Im(\mathscr{D}^{s_1,s_2}))u - \Re(\mathcal{F}^*z_2 - \mathbf{i}\mathscr{D}^{s_1,s_2}\overline{\mathcal{F}^*z_2}), \quad (28c)$$

where $\mathcal{F}^*$ denotes the inverse Fourier transform and $\overline{z}$ denotes the complex conjugate of z, we therefore obtain

$$\left(\mathcal{B}^T\mathcal{B} + \frac{\rho + r_2}{r_3} + \frac{r_1}{r_3}\left(5 + 2\Re(\mathscr{D}^{s_1,s_2}) + 2\Im(\mathscr{D}^{s_1,s_2})\right)\right)u^{m+1}$$
$$= \mathcal{B}^T(p^{m+1} + \frac{q^m}{r_3}) + \frac{1}{r_3}(h + r_2 v^{m+1} - w^m) \quad (29)$$
$$+ \frac{r_1}{r_3}\Re\left(\hat{z}_0^{m+1} + \hat{z}_1^{m+1} + \hat{z}_2^{m+1} + \mathscr{D}^{s_1,s_2}\overline{\hat{z}_1^{m+1}} - i\mathcal{D}^{s_1,s_2}\overline{\hat{z}_2^{m+1}}\right),$$

where $\hat{z}_i^{m+1} = \mathcal{F}^*(z_i^{m+1} + \frac{d_i^m}{r_1})$ for $i = 0, 1, 2$. By updating the Lagrange multipliers, we have the proper solution u. For CDP measurement, one can just refer Eq. (28a) to find the solution. With the linear search of BDCA, the pseudocode of solving model (13) is provided in Algorithm 2. In fact, the proposed method can be applied with other linear operators $\mathcal{A}$, and the derivation is not that different. Here we only verify the effectiveness of the proposed algorithm with two classic measurements.

4.5. **Convergence analysis.** The convergence of the proposed method is studied in this subsection. According to equations (10)-(18), our convergence analysis is mainly based on the following optimization problem

$$\min_{u \in \mathbb{R}^n}\left\{F(u) = G(u) - H(u)\right\}. \quad (30)$$

Both functions $G(u)$ and $H(u)$ in Eq.(14) are strongly convex with modulus $\rho > 0$.

Definition 4.2. For an extended real-valued function $f : \mathbb{R}^n \to \mathbb{R} \cup \{+\infty\}$, the domain of f is the set $\text{dom} f = \{u \in \mathbb{R}^n : F(u) < +\infty\}$. The function f is said to be proper if its domain is nonempty.

The function $H(u)$ is subdifferentiable at every point in $\text{dom}\, H$. The function $G(u)$ is continuously differentiable on an open set containing $\text{dom}\, H$ and

$$\inf_{u \in \mathbb{R}^n} F(u) > -\infty. \quad (31)$$

Under these conditions, the following necessary optimality condition holds.

Proposition 4.3. *(first-order necessary optimality condition* [44]*). If $u^* \in \text{dom}\, F$ is an optimal solution of problem (F), then $\partial H(u^*) = \{\nabla G(u^*)\}$.*

Algorithm 2 BDCA to solve the model (13)

Input: Given parameters r_1, r_2, r_3, λ, β, ρ, $Outmax$, $Intmax$, ϵ_1, ϵ_2 and fixed $\alpha > 0$, $1 > \xi > 0$
Initialize: u^0, $z^0 = \mathcal{A}u^0$, $v^0 = u^0$, $p^0 = \mathcal{B}u^0$, $q^0 = 0$, $w^0 = 0$, $d^0 = 0$
for $k = 1$ **to** $Outmax$ **do**
  Calculate h^k via Eq.(15)
  for $m = 1$ **to** $Intmax$ **do**
    Calculate v^{m+1}, p^{m+1}, z^{m+1}, u^{m+1} via Eq. (20), Eq. (21), Eq. (26), Eq. (29)
    Update multipliers as
    $d^{m+1} = d^m + r_1(z^{m+1} - \mathcal{A}u^{m+1})$
    $w^{m+1} = w^m + r_2(u^{m+1} - v^{m+1})$
    $q^{m+1} = q^m + r_3(p^{m+1} - \mathcal{B}u^{m+1})$
    if $\dfrac{\|u^{m+1} - u^m\|}{\|u^m\|} \leq \epsilon_1$ **then**
      $y^k = u^{m+1}$
    end if
  end for
  Set $d^k = y^k - u^k$
  if $d^k = 0$ **then**
    stop and return u^k
  else
    choose any $\bar{\beta}_k > 0$ and set $\beta_k = \bar{\beta}_k$
    while $F(y^k + \beta_k d^k) > F(y^k) - \alpha\beta_k{}^2\|d^k\|^2$ **do**
      $\beta_k = \xi\beta_k$
    end while
    Set $u^{k+1} = y^k + \beta_k d^k$
    if $u^{k+1} = u^k$ **then**
      stop and return u^k
    end if
  end if
end for

Any point satisfying Proposition 4.3 is called a stationary point of F. In the literature [3], it is shown that $\bar{u}$ is a critical point of F if $\nabla G(\bar{u}) \in \partial H(\bar{u})$. It is obvious that every stationary point u^* is a critical point, but the converse is not true in general.

Theorem 4.4. *For any $u^0 \in \mathbb{R}^n$, either Algorithm 2 returns a critical point of Eq.(16) or generates an infinite sequence such that the following holds.*
(i) $F(u^k)$ is monotonically decreasing and convergent to some F^*.
(ii) Any limit point of u^k is a stationary point of Eq.(16). If in addition F is coercive, then there exists a subsequence of u^k, which converges to a critical point of Eq.(16).
(iii) $\Sigma_{k=0}^{+\infty}\|d^k\|_2^2 < \infty$. Further, if there is some $\bar{\beta}$ such that $\beta_k \leq \bar{\beta}$ for all k, then $\Sigma_{k=0}^{\infty}\|u^{k+1} - u^k\|_2^2 < \infty$.

Proof. If Algorithm 2 stops at the inner iteration and returns u^k, then $u^k = y^k$. Because y^k is the unique solution of the strongly convex problem (16), we have

$$\nabla G\left(y^k\right) = h^k \in \partial H\left(u^k\right), \tag{32}$$

i.e., u^k is a critical point of Eq.(16). Otherwise, by the backtracking process of Algorithm 2, we have

$$F\left(u^{k+1}\right) \le F\left(y^k\right) - \alpha\beta_k^2 \left\|d^k\right\|^2 \le F\left(u^k\right) - \left(\alpha\beta_k^2 + \rho\right)\left\|d^k\right\|^2. \tag{33}$$

In fact, with the strong convexity (Definition 2.3) and y^k is the unique solution of the strongly convex problem (16), the second inequality holds. Therefore, the sequence $\left\{F\left(u^k\right)\right\}$ converges to some F^*, since it is monotonically decreasing and bounded from below by Theorem 31. This proves (i). As a result, we obtain

$$F\left(u^{k+1}\right) - F\left(u^k\right) \to 0, \tag{34}$$

which implies $\left\|d^k\right\|^2 = \left\|y^k - u^k\right\|^2 \to 0$.

If $\bar{u}$ is a limit point of $\left\{u^k\right\}$, there exists a subsequence $\left\{u^{k_i}\right\}$ converging to $\bar{u}$. Then, as $\left\|y^{k_i} - u^{k_i}\right\| \to 0$, we have $y^{k_i} \to \bar{u}$. Since ∇G is continuous, we get

$$h^{k_i} = \nabla G\left(y^{k_i}\right) \to \nabla G(\bar{u}). \tag{35}$$

Hence, we deduce $\nabla G(\bar{u}) \in \partial H(\bar{u})$, thanks to the closedness of the graph of ∂H (see [36], Theorem 24.4). When F is coercive, by (i), the sequence $\left\{u^k\right\}$ must be bounded, which implies the rest of the claim in (ii).

To prove (iii), Eq.(33) implies that

$$\left(\alpha\beta_k^2 + \rho\right)\left\|d^k\right\|^2 \le F(u^k) - F(u^{k+1}). \tag{36}$$

Summing the above inequality from 0 to N,

$$\sum_{k=0}^{N}\left(\alpha\beta_k^2 + \rho\right)\left\|d^k\right\|^2 \le F(u^0) - F(u^{N+1}) \le F(u^0) - \inf_{u\in\mathbb{R}^n} F(u), \tag{37}$$

whence taking the limit when $N \to \infty$, we obtain

$$\sum_{k=0}^{\infty}\rho\|d^k\|_2^2 \le \sum_{k=0}^{\infty}\left(\alpha\beta_k^2 + \rho\right)\left\|d^k\right\|^2 \le F(u^0) - \inf_{u\in\mathbb{R}^n} F(u) < \infty, \tag{38}$$

and $\sum_{k=0}^{\infty}\|d^k\|_2^2 < \infty$. Since

$$u^{k+1} - u^k = y^k - u^k + \beta^k d^k = (1 + \beta^k)d^k, \tag{39}$$

we get

$$\sum_{k=0}^{\infty}\|u^{k+1} - u^k\|_2^2 = \sum_{k=0}^{\infty}(1 + \beta^k)^2\|d^k\|_2^2 \le (1 + \bar{\beta})^2\sum_{k=0}^{\infty}\|d^k\|_2^2 < \infty, \tag{40}$$

and the proof is complete. $\qquad\square$

Remark 4.5. The above considers a general case $\beta_k > 0$, if we choose $\beta_k = \bar{\beta}_k$ for all $k \ge 0$, then condition (iii) of the above Theorem is satisfied and the series $\sum_{k=0}^{\infty}\left\|u^{k+1} - u^k\right\|_2^2$ is finite. Thus, $u^{k+1} - u^k$ is a Cauchy sequence and, hence, convergent.

In addition, the convergence rate on the iterative sequence $\{u^k\}$ is also established in ([3], Theorem 4.9). First, we give the definition of locally Lipschitz continuous. The function F is called Lipschitz continuous if there is some constant $L \geq 0$ such that
$$\|F(x) - F(y)\|_2 \leq L\|x - y\|_2, \quad \forall x, y \in \mathbb{R}^m,$$
and F is said to be locally Lipschitz continuous if, for every x in $\mathbb{R}^m$, there exists a neighborhood U of x such that F restricted to U is Lipschitz continuous. A Lipschitz continuous function must be a locally Lipschitz continuous function.

Next, we show our ∇G is Lipschitz continuous:

$$\|\nabla G(x_1) - \nabla G(x_2)\|_2 \leq \frac{1}{\epsilon}\|x_1 - x_2\|_2 + \lambda\|A^*A\|_2\|x_1 - x_2\|_2 + \rho\|x_1 - x_2\|_2$$
$$= (\frac{1}{\epsilon} + \lambda\|A^*A\|_2 + \rho)\|x_1 - x_2\|_2. \tag{41}$$

Hence ∇G is locally Lipschitz continuous. From the previous assumption, F satisfies the strong KL inequality, and then we know that the following proposition holds.

Proposition 4.6. *Suppose that the sequence $\{u^k\}$ generated by the BDCA has the limit point u^*. Assume that ∇G is locally Lipschitz continuous around u^* and F satisfies the strong Kurdyka-Łojasiewicz inequality at u^* with $\varphi(t) = Mt^{1-\theta}$ for some $M > 0$ and $0 \leq \theta < 1$. Then, the following convergence rates are guaranteed:*
(i) if $\theta = 0$, then the sequences $\{u^k\}$ converges in a finite number of steps to u^*;
(ii) if $\theta \in]0, \frac{1}{2}]$, then the sequences $\{u^k\}$ converges linearly to u^*;
(iii) if $\theta \in]\frac{1}{2}, 1[$, then there exist a positive constant η such that
$$\left\|u^k - u^*\right\|_2 \leq \eta k^{-\frac{1-\theta}{2\theta - 1}},$$
for all large k.

5. **Numerical experiments.** To demonstrate the effectiveness of the proposed regularization model, we present the numerical and visual results in this section. To better simulate the observed image in the real world, the white Gaussian noise with zero mean is added. The Signal-to-noise ratio (SNR) is used for measurement which compares the level of a desired signal to the level of background noise. Denoting $\tilde{b} = |\mathcal{A}u|$ as the degraded image, σ as the noise level, and $\tilde{\zeta}$ as the white Gaussian noise with zero mean, i.e., $b = \tilde{b} + \sigma\tilde{\zeta}$, then the noisy measurement SNR is defined as $\text{SNR}(N, M) = -10\log_{10}\left(\frac{\sum_{j \in \Omega_0, 0 \leq i \leq 2}|b_i(j) - \tilde{b}_i(j)|^2}{\sum_{j \in \Omega_0, 0 \leq i \leq 2}|\tilde{b}_i(j)|^2}\right)$, where $i = 0, 1, 2$, $N = \{\tilde{b}_0, \tilde{b}_1, \tilde{b}_2\}$ is the degraded measurement related to the mask Ω_0 (The masks Ω_i are randomly generated, and we further assume that they are identical, i.e., $\Omega_0 = \Omega_1 = \Omega_2$.) and $M = \{b_0, b_1, b_2\}$ is the ideal measurement. Hence, we have $\sigma = \sqrt{\frac{10^{-\frac{\text{SNR}}{10}}\sum_{0 \leq i \leq 2, j \in \Omega_0}|b_i(j)|^2}{3d}}$, here $d = \#\{j : j \in \Omega_0\}$ counts the number of j. In this paper, different Gaussian noise levels are considered, i.e., $\sigma = 0$, $\sigma = 10$, and $\sigma = 30$. The structural similarity index measure (SSIM) is also applied to quantify reconstruction quality for images. SSIM is defined as

$$\text{SSIM}(x, x^\star) = \frac{(2\mu_x\mu_{x^\star} + C_1)(2\sigma_{xx^\star} + C_2)}{(\mu_x^2 + \mu_{x^\star}^2 + C_1)(\sigma_x^2 + \sigma_{x^\star}^2 + C_2)}, \tag{42}$$

where μ_x, μ_{x^*} and σ_x, $\sigma_{x^\star}$, $\sigma_{xx^\star}$ are the mean and the standard deviation of x and x^*, respectively. The positive constants C_1 and C_2 are used to avoid a null denominator, which is defaulted by the Matlab built-in ssim function.

(a) Numerical results of $\Phi(u) = \|\nabla u\|_1$.

(b) Corresponding average visual result.

(c) Numerical results of $\Phi(u) = \|\mathcal{W}u\|_1$.
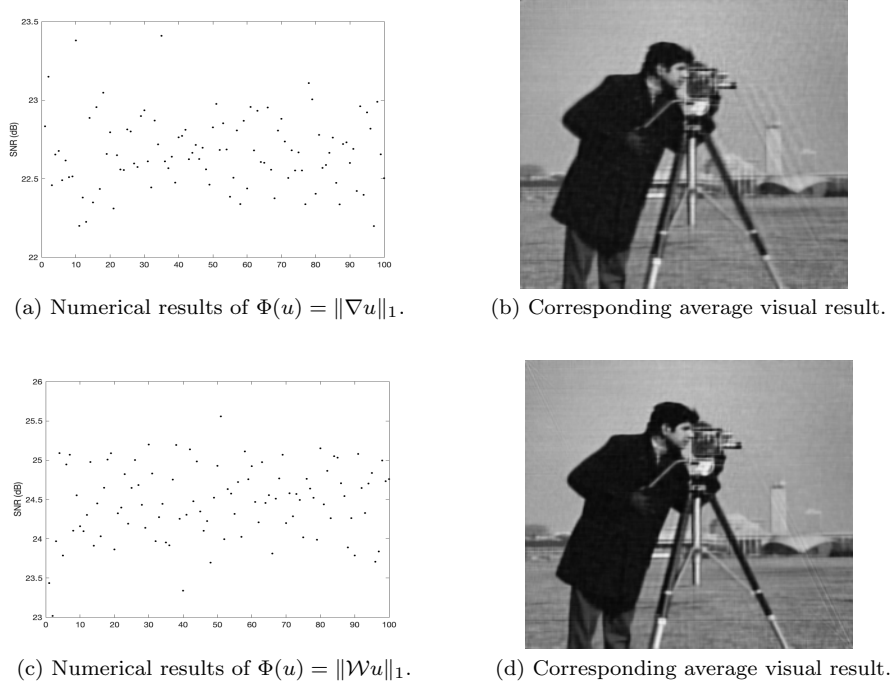

(d) Corresponding average visual result.

FIGURE 1. The sensitive analysis of initial values. The proposed model (10) of the image 'cameraman' with the degradation of the $3n$ Fourier mask ratio 50% and SNR = 30. (a) SNR(dB) results with 100 random values of $\Phi(u) = \|\nabla u\|_1$; (c) SNR(dB) results with 100 random values of $\Phi(u) = \|\mathcal{W}u\|_1$; the average visual results with (b) SNR = 22.67 and (d) SNR = 24.47.
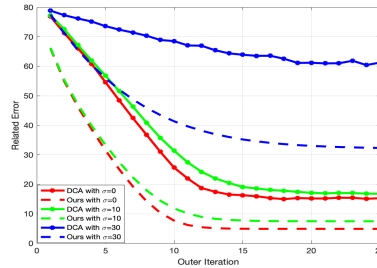

FIGURE 2. Comparisons between our BDCA and DC algorithm of Image 'cameraman' with CDP mask type $J = 2$. Here the red, green, and blue lines are with $\sigma = 0$, $\sigma = 10$, and $\sigma = 30$ respectively.

Before comparing with other methods, we first conduct parameter analysis and convergence analysis with Eq.(3) of our approach.

5.1. **Parameter setting.** In this subsection, the initialization and parameter sensitivity analyses are presented. Since model (10) is non-convex, the initial value has
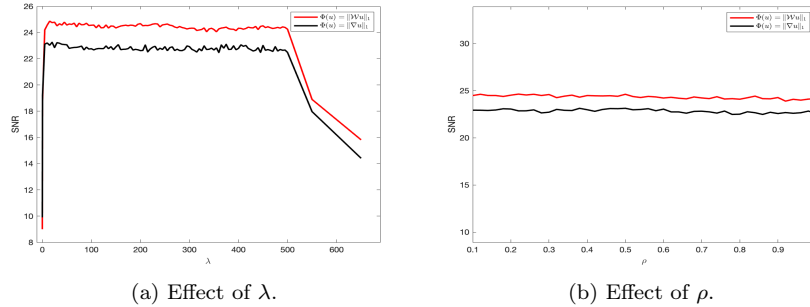
(a) Effect of λ.

(b) Effect of ρ.

FIGURE 3. Sensitive analysis with parameters λ, ρ. Image 'cameraman' with the degradation of the $3n$ Fourier mask ratio 50% and SNR $= 30$.

(a) Effect of r_1.

(b) Effect of r_2.

(c) Effect of r_3.

(d) Effect of r_1.
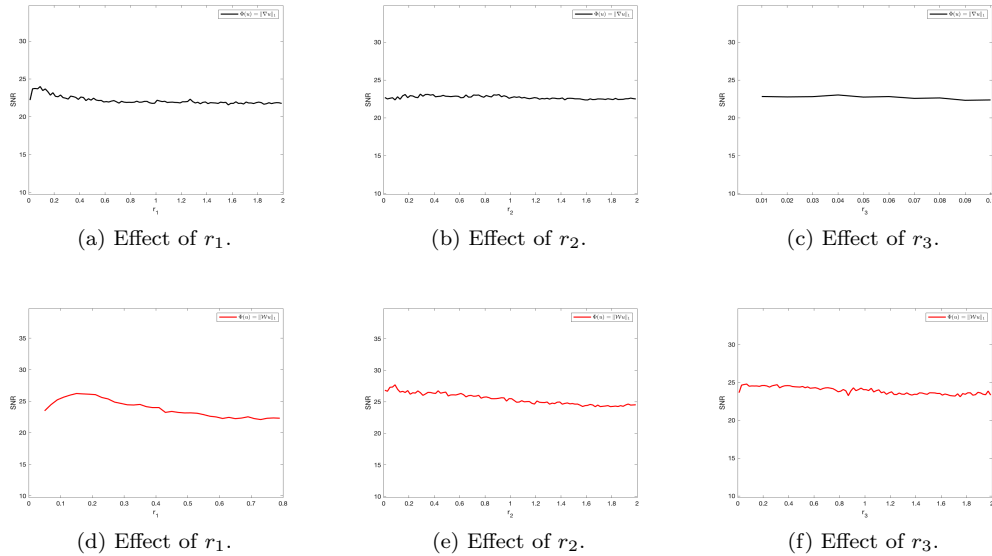
(e) Effect of r_2.

(f) Effect of r_3.

FIGURE 4. Sensitive analysis with parameters r_1, r_2, and r_3. Image 'cameraman' with the degradation of the $3n$ Fourier mask ratio 50% and SNR $= 30$. The first row displays the results of the proposed model with $\Phi(u) = \|\nabla u\|_1$ and the second row is the results of the proposed model with $\Phi(u) = \|\mathcal{W}u\|_1$.

some effects on the final result. We analyze the effectiveness of 100 random initial values. In Algorithm 2, according to the DFT Eq.(1), we set

$$z_i^0(\omega) = \begin{cases} b_i(\omega)\exp\left(-2\pi\mathbf{i}\theta_i\omega\right), & \text{if } \omega \in \Omega, \\ 0, & \text{otherwise,} \end{cases} \tag{43}$$

and $v^0 = \mathcal{F}^*z_1^0$ as initial values. Thus, by giving b_i and ω, all we need to change is the θ_i. To test the sensitivity of the final result to the initial value, we set θ_i as random values. Cropped by the sampling masks w.r.t. undersampling ratios 50% (mask ratio 50%) and the SNR 30, we test the degraded image 'cameraman'

with 100 random initial values. The test results are displayed in Fig. 1, which demonstrates the robustness of the proposed method with random initialization. In numerical results of the case $\Phi(u) = \|\nabla u\|_1$ (Fig. 1 (a)), SNR falls into the interval $[22.20, 23.41]$ with the average value equal to 22.67, the corresponding average result is shown in Fig. 1 (b) with parameters are set as $\lambda = 100$, $\rho = 0.1$, $r_1 = 0.2$, $r_2 = 0.3$, $r_3 = 0.02$. For $\Phi(u) = \|\mathcal{W}u\|_1$, SNR $\in [23.02, 25.56]$ and the average value is 24.47, the corresponding average results are presented in Fig. 1 (d) (parameters are set as $\lambda = 100$, $\rho = 0.5$, $r_1 = 0.3$, $r_2 = 1.5$, $r_3 = 0.1$).

As we reviewed in Section 3, the boost DC algorithm (BDCA) is the extension of DC algorithm (DCA). As we proposed to handle the phase retrieval task with BDCA, Fig. 2 presents the related error curves of BDCA and DCA to further demonstrate the advantages of the proposed scheme. We test the phase retrieval with TV regularizer on the image 'cameraman' with CDP mask type $J = 2$ with different noise levels $\sigma = 0$ (red lines), $\sigma = 10$ (green lines), and $\sigma = 30$ (blue lines). For example, the green lines are the reconstruction results obtained when the image degradation with the CDP mask and noise level $\sigma = 10$. From the two curves, we can see that the relative error of the proposed method decreases faster, and finally, a small error result is obtained. That is, a better reconstruction result is obtained. Through testing on three different noise levels, we can see that our method also has good stability with the CDP mask. It is worth mentioning that the results in Fig. 2 are also based on random initial values. In particular, we use Matlab's built-in random function and fix the random value as 2022 with the random seed. Both Fig. 1 and Fig. 2 illustrate the stability of our method.

Fig. 1 illustrates that the proposed model is robust to random initialization. However, the recovery result is also decided by the parameters. The parameter analysis of the proposed model is as follows. First of all, we analyze the balance parameter λ in the proposed model Eq.(10) by fixing the other parameters, *i.e.*, $\rho = 0.1$, $r_1 = 0.2$, $r_2 = 0.3$, $r_3 = 0.02$ for $\Phi(u) = \|\nabla u\|_1$ and $\rho = 0.5$, $r_1 = 0.3$, $r_2 = 1.5$, $r_3 = 0.1$ for $\Phi(u) = \|\mathcal{W}u\|_1$. We test λ ranging from 5 to 500 with the step size 5. Besides, we add the results with $\lambda = 0.1, 0.5$ and $\lambda = 550, 650$. With the fixed initial parameters, which are also generated by random, 100 results with respect to different λ are obtained in Fig. 3 (a). From the curves, we can see that the proposed models are stable with parameter λ in some range, but when we enlarge the range, the performance of the proposed algorithms will decrease. Then we research the influence of the positive constant ρ, which makes sure the strong convexity of $H(x)$ and $G(x)$. We set $\rho \in [0.1, 1]$ and the step-size as 0.02, and the effect of ρ is exhibited in Fig. 3 (b). Finally, the Lagrange penalty parameters r_1, r_2, and r_3 are studied. Since parameters r_1, r_2, and r_3 lead to relatively poor results under some values, we exhibit the results of two regularizers in Fig. 4, respectively. We set $r_1, r_2, r_3 \in [0.01, 2]$ with step-size 0.02 and the results are displayed in Fig. 4. As the results of r_3 with $\Phi(u) = \|\nabla u\|_1$ are relatively poor in $r_3 > 0.11$ and r_1 with $\Phi(u) = \|\mathcal{W}u\|_1$ are relatively poor in $r_1 > 0.8$, so we set $r_3 \in [0.01, 0.1]$ with step-size 0.01 in Fig. 4 (c) and $r_1 \in [0.05, 0.79]$ with step-size 0.02 in Fig. 4 (d). From Fig. 3 and Fig. 4, the proposed model has good robustness in different parameters.

5.2. **Convergence behavior.** In this subsection, we present the convergence behavior of the proposed scheme in terms of experimental results. In Fig. 5, the energy and the corresponding relative error with respect to the inner iteration of $\Phi(u) = \|\nabla u\|_1$ and $\Phi(u) = \|\mathcal{W}u\|_1$ are given. It can be seen from the graph that our
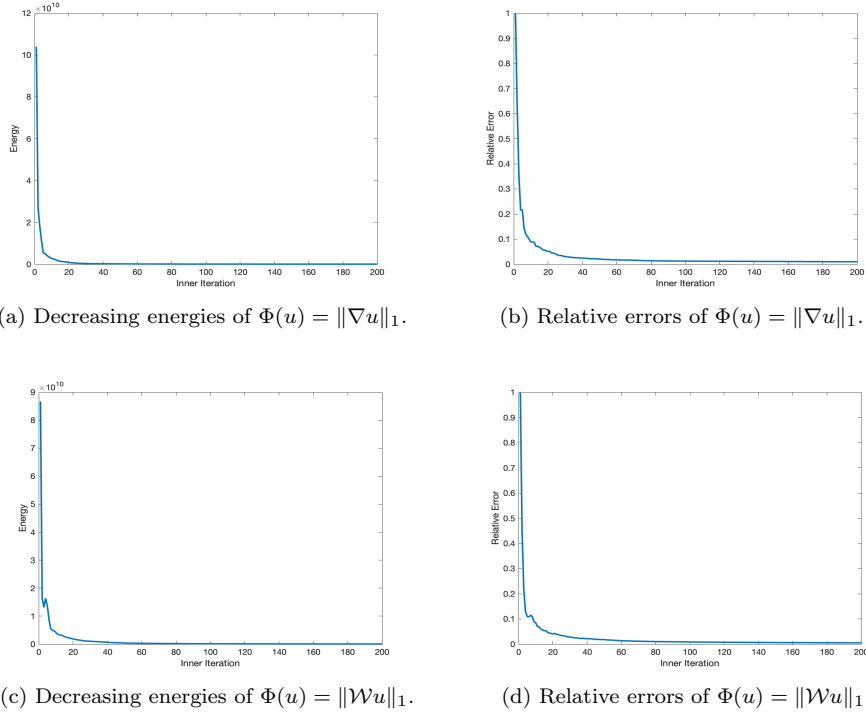
(a) Decreasing energies of $\Phi(u) = \|\nabla u\|_1$.

(b) Relative errors of $\Phi(u) = \|\nabla u\|_1$.

(c) Decreasing energies of $\Phi(u) = \|\mathcal{W}u\|_1$.

(d) Relative errors of $\Phi(u) = \|\mathcal{W}u\|_1$.

FIGURE 5. The convergence behavior of the proposed model (10) of the image 'cameraman' with the degradation of the $3n$ Fourier mask ratio 50% and SNR = 30.

(a) Original   (b) TVB [11] (29.05/0.7481)(c) Our TV (30.63/0.8115)(d) Our TF (32.96/0.9342)
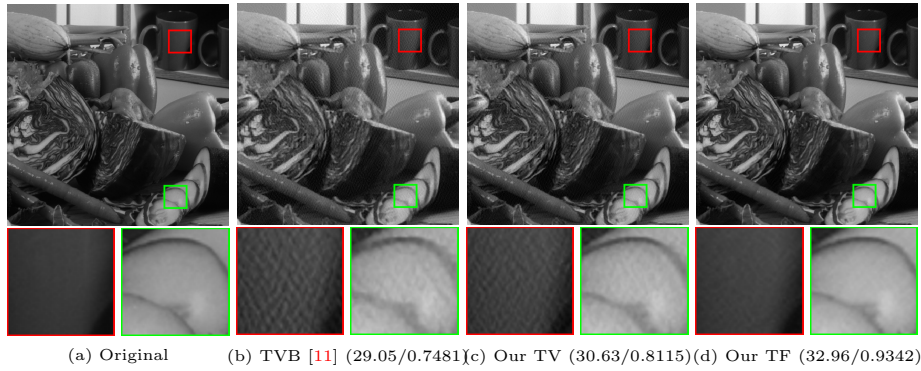
FIGURE 6. The comparison results (SNR/SSIM) of Img10 with $3n$ Fourier mask ratio 50% and $\sigma = 0$.

method is convergent. After 40 and 80 iterations, the objective function reaches the minimum with regularizers $\Phi(u) = \|\nabla u\|_1$ and $\Phi(u) = \|\mathcal{W}u\|_1$, respectively. The energy graph and the relative error graph also manifest the correctness of Theorem 4.4.

5.3. **Phase retrieval results.** In this subsection, the comparison results of different phase retrieval methods are studied. We compare the proposed method with

(a) Original   (b) TVB [11] (24.42/0.5375) (c) Our TV (25.76/0.6035) (d) Our TF (26.99/0.7715)
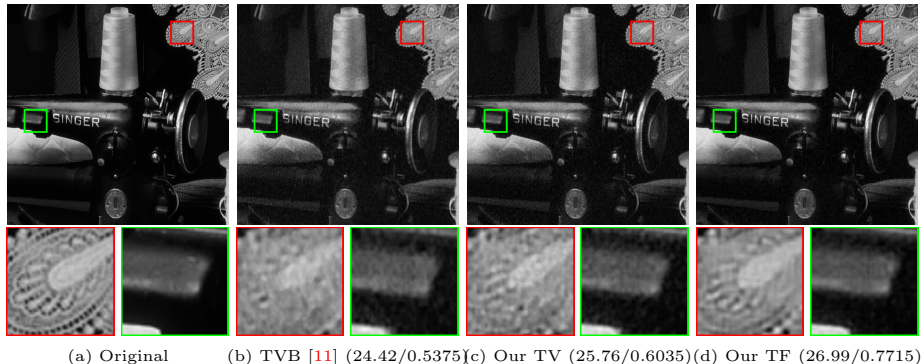
FIGURE 7. The comparison results (SNR/SSIM) of Img08 with $3n$ Fourier mask ratio 50% and $\sigma = 10$.

TABLE 1. Average results of Set18 with SNR/SSIM/running time in second of phase retrieval (3n Fourier measurements).

mask 50%	TVB [11]	Our TV	Our TF
$\sigma = 0$	27.83/0.7411/$\underline{24.12}$	$\underline{27.99}$/$\underline{0.7755}$/**21.80**	**28.97**/**0.7952**/60.33
$\sigma = 10$	23.14/0.5472/$\underline{24.37}$	$\underline{24.00}$/$\underline{0.5616}$/**19.70**	**24.59**/**0.6148**/57.28
$\sigma = 30$	19.40/0.4117/$\underline{24.70}$	$\underline{20.08}$/$\underline{0.4365}$/**19.93**	**21.27**/**0.4677**/60.17

some state-of-the-art methods of phase retrieval. However, due to the different measurements, we compare the proposed method with TVB [11] under mask Eq.(3), and the proposed model with RAAR [30], RAF [48], RWF [52], TAF [47], CDA [54], HIO [19], TWF [15], WF [9] and DDWF [34] with DCP measurement Eq.(4). All the experiments[1] are conducted in MATLAB R2020a under macOS Catalina 10.15.4 with a 1.40GHz CPU and 8GB memory. We test 18 images of size 500×500 from Set18[2]. Two different measurements ($3n$ Fourier measurement and DCP) with different Gaussian noise levels $\sigma = 0$, $\sigma = 10$, and $\sigma = 30$ are studied.

Firstly, we consider the $3n$ Fourier measurement Eq.(3) under mask ratios 50% and $\sigma = 0$, $\sigma = 10$, and $\sigma = 30$. The results are displayed in Fig. 6 and Fig. 7, which demonstrate the advantages of the proposed model. The average results of Set18 with SNR, SSIM and running time in second are shown in Table 1. The best numerical result is in bold, and the second-best result is underlined. We can see from the numerical results that the proposed method has better results than the TVB method [11].

Secondly, the CDP mask Eq.(4) is considered. In addition to the above comparison, the classical phased retrieval methods Kacz [50], PhaseLift [7], PhaseMax [4], PhaseLamp [16], SketchyCGM [53] are considered in Fig. 8. The initial value u^0 was generated by the error reduction (ER) [21] method with 40 iterations. The comparison results of visual quality and numerical SNR and SSIM results are displayed in Fig. 9 and Fig. 10 with $\sigma = 10$ and $\sigma = 30$, respectively. The results of our TV and our TF illustrate that the proposed method can well handle the phase retrieval problem with the CDP mask. The average results of compared methods

---

[1]The codes of TVB were provided by the corresponding author, other methods' codes are from the PhasePack [10] (https://github.com/tomgoldstein/phasepack-matlab).

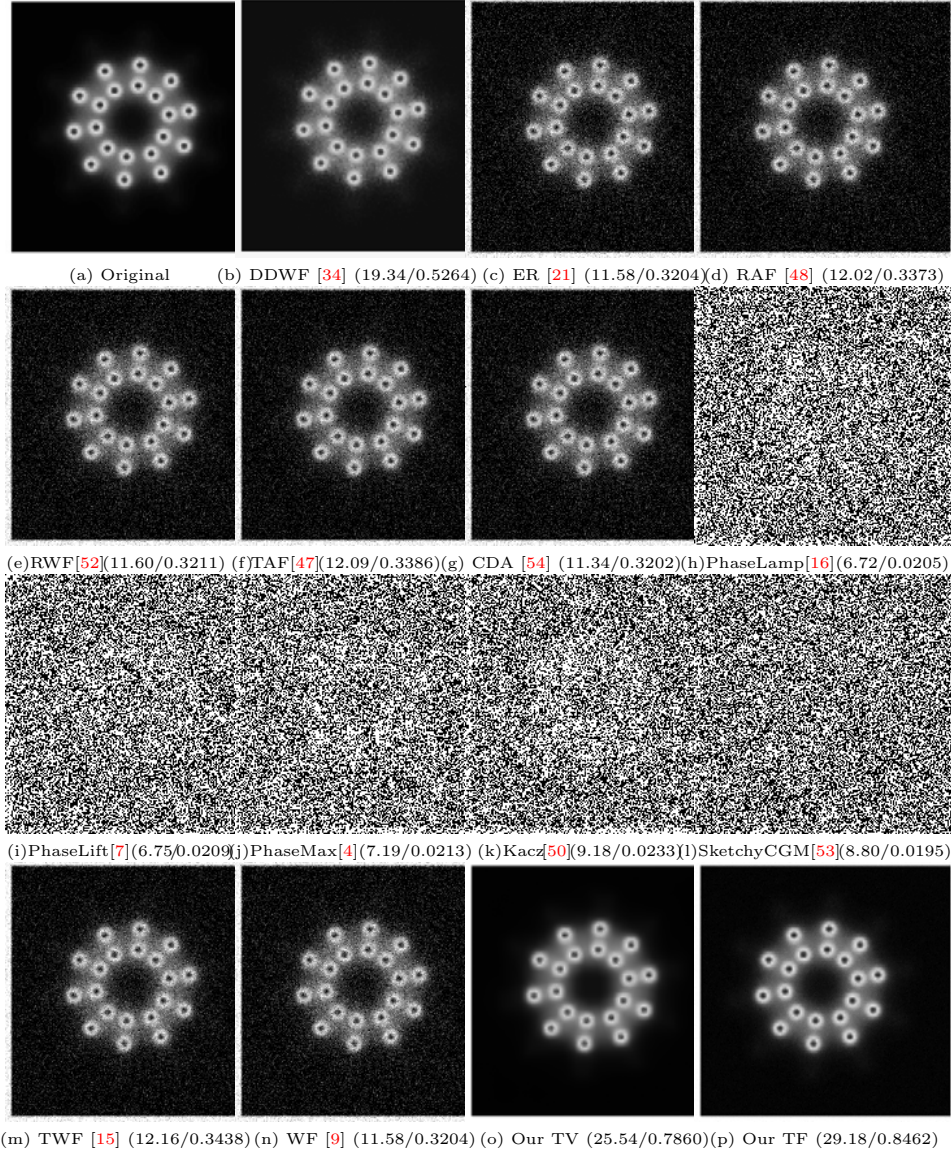[2]https://github.com/cszn/IRCNN/tree/master/testsets/Set18

FIGURE 8. The comparison results (SNR/SSIM) of (2D projection slice of molecule) with CDP mask type $J = 2$ and $\sigma = 1$.

are shown in Table 2, which demonstrates our method has the best performance. Besides, the average running time in the second of the compared methods is listed in Table 3, in which those methods without regularizer have less time-consuming. But from both the reconstruction results and the time consumption, we can see that the proposed methods have a better balance. Furthermore, combining the average running time listed in Table 1, we can see that our methods still have the advantage of time consumption. From the compared results of the DDWF [34], *i.e.*, for the kind of image (2D projection slices of the caffeine molecule) in Fig. 8, we also have better phase retrieval results.

(a) Original   (b) ER [21] (25.13/0.6142)(c) RAAR [30] (25.13/0.6143)(d) RAF [48] (25.13/0.6142)

(e) RWF [52] (25.13/0.6142)(f) TAF [47] (24.62/0.6140)(g) CDA [54] (25.00/0.6137)(h) HIO [19] (14.28/0.1777)

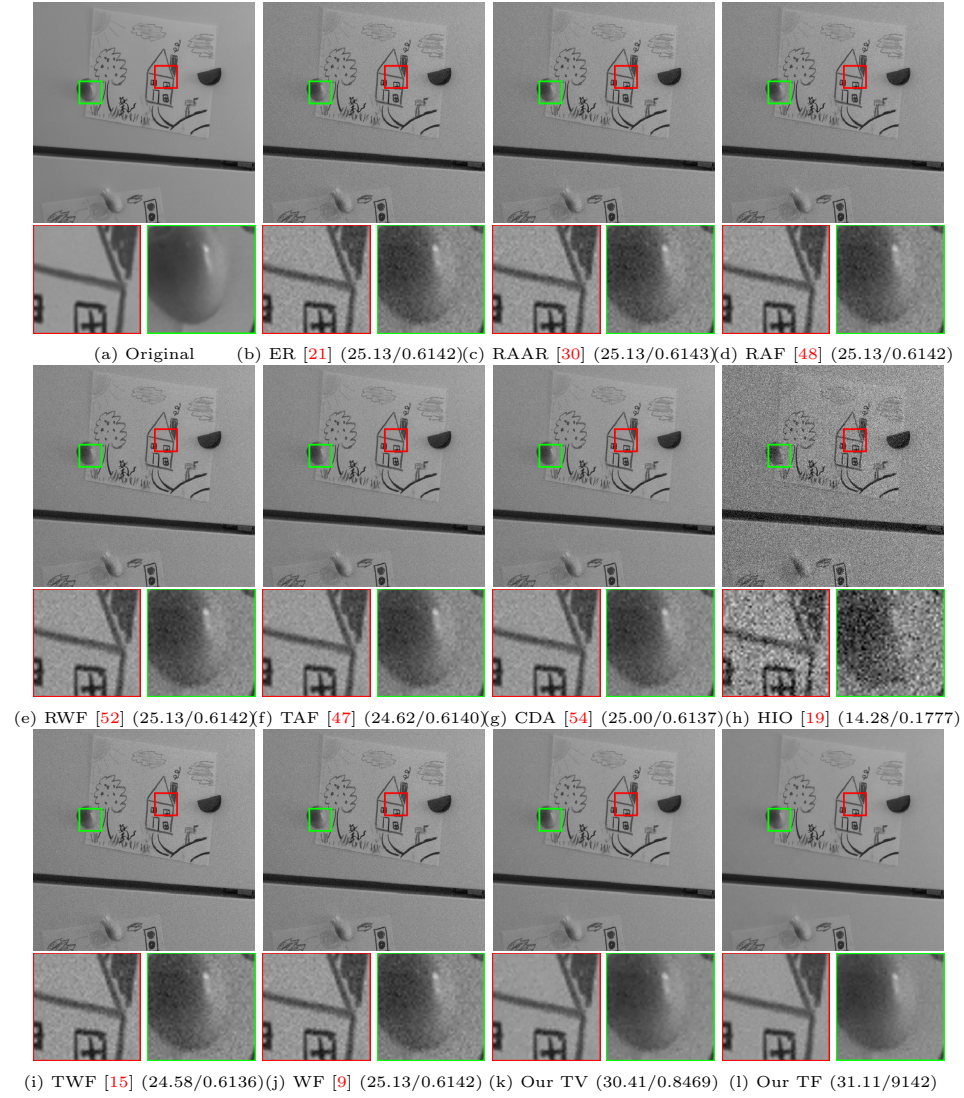(i) TWF [15] (24.58/0.6136)(j) WF [9] (25.13/0.6142) (k) Our TV (30.41/0.8469) (l) Our TF (31.11/9142)

FIGURE 9. The comparison results (SNR/SSIM) of Img13 with CDP mask type $J = 2$ and $\sigma = 10$.

To further demonstrate the effectiveness of the proposed algorithm, we present the ablation experiment in Figure 11. We first set the initial value with the Matlab pseudorandom values generator 'rand(m, n)', where m and n are the sizes of an image. We fix the random seed as 2022 to ensure every experiment with the exact same random value. The degradation is with CDP mask type $J = 2$ and noise level $\sigma = 10$. From the previously compared results and Figure 11 (c), (d), and (e), we can see that the RAF, TAF, and TWF methods are sensitive to initial values. However, our methods (h) and (i) still have competitive reconstruction results. On the other hand, the proposed methods contain regularizers, but most of the compared algorithms are only with the data fidelity term. Here we set the
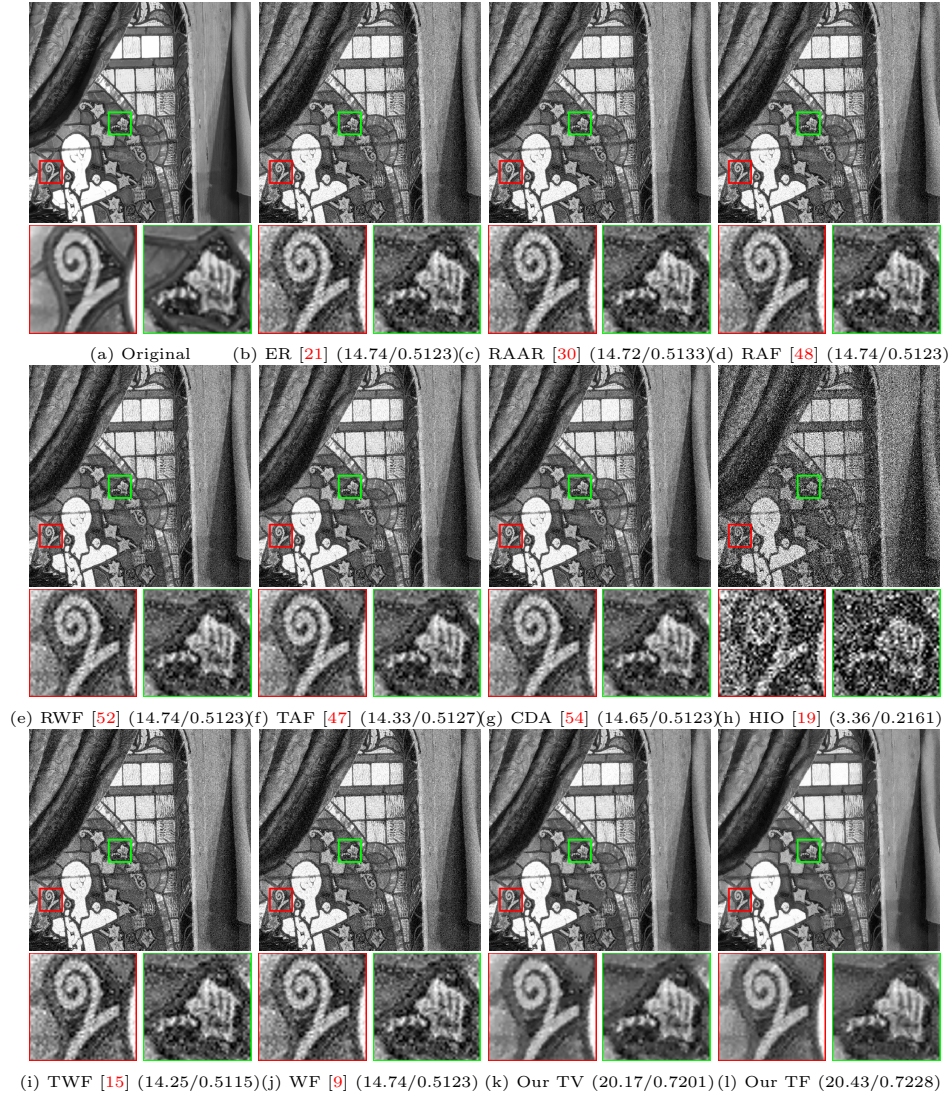
(a) Original   (b) ER [21] (14.74/0.5123)(c) RAAR [30] (14.72/0.5133)(d) RAF [48] (14.74/0.5123)

(e) RWF [52] (14.74/0.5123)(f) TAF [47] (14.33/0.5127)(g) CDA [54] (14.65/0.5123)(h) HIO [19] (3.36/0.2161)

(i) TWF [15] (14.25/0.5115)(j) WF [9] (14.74/0.5123) (k) Our TV (20.17/0.7201)(l) Our TF (20.43/0.7228)

FIGURE 10. The comparison results (SNR/SSIM) of Img03 with CDP mask type $J = 2$ and $\sigma = 30$.

parameter λ in the proposed model (10) as $1e30$. We recall the proposed model

$$\min_{0 \leq u \leq 1} F(u) = \min_{0 \leq u \leq 1} \frac{\lambda}{2} \|| \mathcal{A}u| - b\|^2 + \Phi(u),$$

where $\lambda = 1e30$ means the regularizer can almost be neglected. Hence it would be fairer to compare our model with those methods only with the data fidelity term. From Fig. 11 (f) and (g), we can see that the results of our models still have outperformed results.

6. **Conclusions.** In this paper, we propose a regularization framework to reconstruct the image from the observation that is corrupted by the heavy noise effectively. For the non-convex minimization problem, it is difficult to find a robust

(a) Original   (b) Random ini (3.48/0.0577)   (c) RAF [48] (4.68/0.1271)

(d) TAF [47] (4.85/0.1232)   (e) TWF [15] (5.10/0.1171)   (f) Our TV-0 (21.52/0.5732)

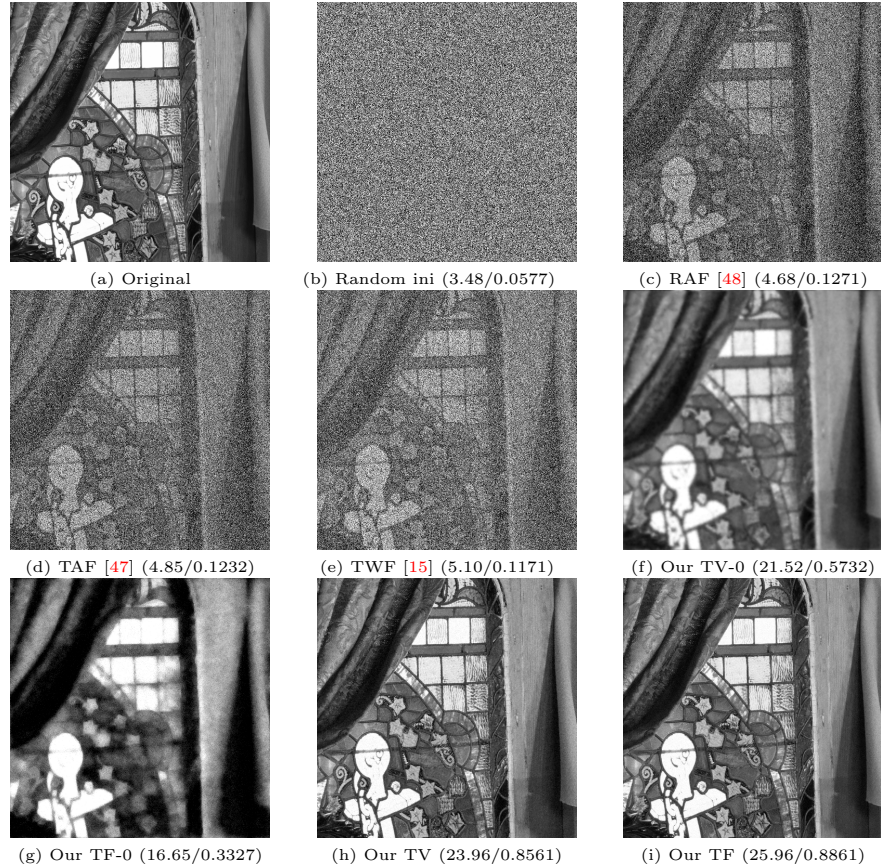(g) Our TF-0 (16.65/0.3327)   (h) Our TV (23.96/0.8561)   (i) Our TF (25.96/0.8861)

FIGURE 11. The comparison results (SNR/SSIM) with random initial value of (2D projection slice of molecule) with CDP mask type $J = 2$ and $\sigma = 10$. (a) the original image; (b) The random value image with Matlab command 'u0=rand(m, n)'; (c) RAF [48]; (d) TAF [47]; (e) TWF [15]; (f) Our TV with parameter $\lambda = 1e30$; (g) Our TF with parameter $\lambda = 1e30$; (h) Our TV; (i) Our TF.

TABLE 2. Average results of Set18 with SNR/SSIM of phase retrieval (CDP measurement with $J = 2$).

CDP mask	ER [21]	RAAR [30]	RAF [48]	RWF [52]	TAF [47]	CDA [54]	HIO [19]	TWF [15]	WF [9]	Our TV	Our TF
$\sigma = 30$	22.55/0.3406	22.94/0.3432	22.55/0.3408	22.55/0.3406	22.16/0.3418	21.72/0.3404	12.59/0.1212	22.03/0.3394	22.55/0.3406	<u>27.02</u>/<u>0.6292</u>	**27.11/0.6406**
$\sigma = 10$	30.16/0.7323	30.56/0.7490	30.16/0.7324	30.16/0.7323	30.21/0.7345	30.06/0.7315	20.63/0.3424	30.20/0.7042	29.04/0.7402	<u>34.53</u>/<u>0.8902</u>	**35.29/0.9002**

minimizer. By reformulating the proposed model with the Huber function and the square term, the non-convex model can be solved by the boosted DC algorithm with the convergence guarantee. To better demonstrate the robustness and flexibility of the proposed framework, two general measurements are used to describe the degradation process and the two regularizers are tested. Both tight frame and total variation terms have reasonable convergence rates in handling the phase retrieval task, which illustrates the robustness of the proposed framelet model. In addition, we present the theoretical analysis of our model. The numerical results of

TABLE 3.   Average running time in second of Set18 of phase retrieval (CDP measurement with $J = 2$).

CDP mask	ER [21]	RAAR [30]	RAF [48]	RWF [52]	TAF [47]	CDA [54]	HIO [19]	TWF [15]	WF [9]	Our TV	Our TF
$\sigma = 30$	0.67	3.20	2.83	14.39	2.91	1.55	3.42	3.06	154.91	62.77	75.09
$\sigma = 10$	0.66	3.06	2.75	10.61	2.81	1.27	2.92	3.01	136.06	61.21	73.85

our method on both measurements also give a positive demonstration. Compared to other methods, the proposed model achieves superior performances in both numerical and visual results.

REFERENCES

[1] L. T. H. An and P. D. Tao, The DC (difference of convex functions) programming and DCA revisited with DC models of real world nonconvex optimization problems, *Annals of Operations Research*, **133** (2005), 23-46.

[2] F. J. A. Artacho, R. M. Fleming and P. T. Vuong, Accelerating the DC algorithm for smooth functions, *Mathematical Programming*, **169** (2018), 95-118.

[3] F. J. A. Artacho and P. T. Vuong, The boosted difference of convex functions algorithm for nonsmooth functions, *SIAM Journal on Optimization*, **30** (2020), 980-1006.

[4] S. Bahmani and J. Romberg, Phase retrieval meets statistical learning theory: A flexible convex relaxation, *Electron. J. Stat.*, **11** (2017), 5254-5281.

[5] S. Boyd, S. P. Boyd, and L. Vandenberghe, *Convex Optimization*, Cambridge University Press, Cambridge, 2004.

[6] J. F. Cai, H. Liu and Y. Wang, Fast rank-one alternating minimization algorithm for phase retrieval, *J. Sci. Comput.*, **79** (2019), 128-147.

[7] E. J. Candés, Y. C. Eldar, T. Strohmer and V. Voroninski, Phase retrieval via matrix completion, *SIAM Review*, **57** (2015), 225-251.

[8] E. J. Candés, X. Li and M. Soltanolkotabi, Phase retrieval from coded diffraction patterns, *Appl. Comput. Harmon. Anal.*, **39** (2015), 277-299.

[9] E. J. Candés, X. Li and M. Soltanolkotabi, Phase retrieval via Wirtinger flow: Theory and algorithms, *IEEE Trans. Inform. Theory*, **61** (2015), 1985-2007.

[10] R. Chandra, T. Goldstein and C. Studer, Phasepack: A phase retrieval library, *2019 13th International Conference on Sampling Theory and Applications* , (2019), 1-5.

[11] H. Chang, Y. Lou, M. K. Ng and T. Zeng, Phase retrieval from incomplete magnitude information via total variation regularization, *SIAM Journal on Scientific Computing*, **38** (2016), 3672-A3695.

[12] B. Chen, Z. Zhang, D. Xia, E. Y. Sidky and X. Pan, Non-convex primal-dual algorithm for image reconstruction in spectral CT, *Computerized Medical Imaging and Graphics*, **87** (2021), 101821.

[13] L. Chen, D. Sun and K. C. Toh, A note on the convergence of admm for linearly constrained convex optimization problems, *Computational Optimization and Applications*, **66** (2017), 327-343.

[14] P. Chen, A. Fannjiang and G. R. Liu, Phase retrieval with one or two diffraction patterns by alternating projections with the null initialization, *J. Fourier Anal. Appl.*, **24** (2018), 719-758.

[15] Y. Chen and E. J. Candés, Solving random quadratic systems of equations is nearly as easy as solving linear systems, *Communications on Pure and Applied Mathematics*, **70** (2017), 822-883.

[16] O. Dhifallah, C. Thrampoulidis and Y. M. Lu, Phase retrieval via polytope optimization: Geometry, phase transitions, and new algorithms, preprint, arXiv:1805.09555, 2018.

[17] Y. C. Eldar, P. Sidorenko, D. G. Mixon, S. Barel and O. Cohen, Sparse phase retrieval from short-time Fourier measurements, *IEEE Signal Processing Letters*, **22** (2014), 638-642.

[18] V. Elser, Phase retrieval by iterated projections, *Journal of the Optical Society of America. A*, **20** (2003), 40-55.

[19] J. R. Fienup, Phase retrieval algorithms: A comparison, *Applied Optics*, **21** (1982), 2758-2769.

[20] D. Gabay and B. Mercier, A dual algorithm for the solution of nonlinear variational problems via finite element approximation, *Computers & Mathematics with Applications*, **2** (1976), 17-40.

[21] R. W. Gerchberg and W. O. A. Saxton, A practical algorithm for the determination of phase from image and diffraction plane pictures, *Optik*, **35** (1972), 237-246.

[22] R. A. Gonsalves, Phase retrieval and diversity in adaptive optics, *Optical Engineering*, **21** (1982), 215829.

[23] L. T. Hoai An, An efficient algorithm for globally minimizing a quadratic function under convex quadratic constraints, *Mathematical Programming*, **87** (2000), 401-426.

[24] P. J. Huber, Robust regression: Asymptotics, conjectures and Monte Carlo, *Ann. Statist.*, **1** (1973), 799-821.

[25] X. Ji and X. Liu, Inverse electromagnetic source scattering problems with multifrequency sparse phased and phaseless far field data, *SIAM J. Sci. Comput.*, **41** (2019), 1368-1388.

[26] M. V. Klibanov, P. E. Sacks and A. V. Tikhonravov, The phase retrieval problem, *Inverse Problems*, **11** (1995), 1-28.

[27] C. Kümmerle, C. Mayrink Verdun and D. Stöger, Iteratively reweighted least squares for basis pursuit with global linear convergence rate, *Advances in Neural Information Processing Systems*, **34** (2021), 2873-2886.

[28] C. Lemaréchal and C. Sagastizábal, Practical aspects of the Moreau–Yosida regularization: Theoretical preliminaries, *SIAM Journal on Optimization*, **7** (1997), 367-385.

[29] K. Liu, J. Wang, Z. Xing, L. Yang and J. Fang, Low-rank phase retrieval via variational Bayesian learning, *IEEE Access*, **7** (2018), 5642-5648.

[30] D. R. Luke, Relaxed averaged alternating reflections for diffraction imaging, *Inverse Problems*, **21** (2005), 37-50.

[31] F. Meng, D. Sun and G. Zhao, Semismoothness of solutions to generalized equations and the Moreau-Yosida regularization, *Mathematical Programming*, **104** (2005), 561-581.

[32] R. Mifflin, L. Qi and D. Sun, Properties of the Moreau-Yosida regularization of a piecewise C^2 convex function, *Mathematical Programming*, **84** (1999), 269-281.

[33] P. Netrapalli, P. Jain and S. Sanghavi, Phase retrieval using alternating minimization, *IEEE Transactions on Signal Processing*, **63** (2015), 4814-4826.

[34] T. Pang, Q. Li, Z. Wen and Z. Shen, Phase retrieval: A data-driven wavelet frame based approach, *Applied and Computational Harmonic Analysis*, **49** (2020), 971-1000.

[35] T. Qiu, P. Babu and D. P. Palomar, PRIME: Phase retrieval via majorization-minimization, *IEEE Trans. Signal Process.*, **64** (2016), 5174-5186.

[36] R. T. Rockafellar, *Convex Analysis*, Princeton University Press, Princeton, N.J., 1970..

[37] L. I. Rudin, S. Osher and E. Fatemi, Nonlinear total variation based noise removal algorithms, *Physica D: Nonlinear Phenomena*, **60** (1992), 259-268.

[38] T. Schüle, C. Schnörr, S. Weber and J. Hornegger, Discrete tomography by convex-concave regularization and DC programming, *Discrete Applied Mathematics*, **151** (2005), 229-243.

[39] Y. Shechtman, Y. C. Eldar, O. Cohen, H. N. Chapman, J. Miao and M. Segev, Phase retrieval with application to optical imaging: A contemporary overview, *IEEE Signal Processing Magazine*, **32** (2015), 87-109.

[40] B. Shi, Q. Lian and S. Chen, Sparse representation utilizing tight frame for phase retrieval, *EURASIP Journal on Advances in Signal Processing*, **2015** (2015), 1-11.

[41] W. Shu Lin and T. Zhou, Convergence analysis for three parareal solvers, *SIAM Journal on Scientific Computing*, **37** (2015), 970-992.

[42] P. D. Tao, Algorithms for solving a class of nonconvex optimization problems. methods of subgradients, *in North-Holland Mathematics Studies*, **129** (1986), 249-271.

[43] P. D. Tao and L. T. H. An, Convex analysis approach to DC programming: Theory, algorithms and applications, *Acta Mathematica Vietnamica*, **22** (1997), 289-355.

[44] J. F. Toland, On subdifferential calculus and duality in nonconvex optimization, *Bulletin Des Sciences Mathématiques*, **60** (1979), 177-183.

[45] J. A. Tropp, A. Yurtsever, M. Udell and V. Cevher, Streaming low-rank matrix approximation with an application to scientific simulation, *SIAM Journal on Scientific Computing*, **41** (2019), 2430-2463.

[46] N. Vaswani, S. Nayer and Y. C. Eldar, Low-rank phase retrieval, *IEEE Transactions on Signal Processing*, **65** (2017), 4059-4074.

[47] G. Wang, G. Giannakis and Y. C. Eldar, Solving systems of random quadratic equations via truncated amplitude flow, *IEEE Transactions on Information Theory*, **64** (2018), 773-794.

[48] G. Wang, G. B. Giannakis, Y. Saad and J. Chen, Solving almost all systems of random quadratic equations, preprint, `arXiv:1705.10407`, 2017.

[49] G. Wang, L. Zhang, G. B. Giannakis, M. Akçakaya and J. Chen, Sparse phase retrieval via truncated amplitude flow, *IEEE Transactions on Signal Processing*, **66** (2018), 479-491.

[50] K. Wei, Solving systems of phaseless equations via Kaczmarz methods: A proof of concept study, *Inverse Problems*, **31** (2015), 125008.

[51] J. Xiao, M. K. Ng and Y. Yang, On the convergence of nonconvex minimization methods for image recovery, *IEEE Transactions on Image Processing*, **24** (2015), 1587-1598.

[52] Z. Yuan and H. Wang, Phase retrieval via reweighted Wirtinger flow, *J. Comput. Appl. Math.,* **355** (2019), 162-173.

[53] A. Yurtsever, M. Udell, J. Tropp and V. Cevher, Sketchy decisions: Convex low-rank matrix optimization with optimal storage, *Artificial Intelligence and Statistics*, (2017), 1188-1196.

[54] W. J. Zeng and H. So, Coordinate descent algorithms for phase retrieval, *Signal Processing*, **169** (2019), 107418.

[55] S. Zhang, Absolute phase retrieval methods for digital fringe projection profilometry: A review, *Optics and Lasers in Engineering*, **107** (2018), 28-37.

[56] W. Zhou, J. F. Cai and H. Gao, Adaptive tight frame based medical image reconstruction: A proof-of-concept study for computed tomography, *Inverse Problems*, **29** (2013), 125006.